J. Fluid Mech. (1989), *vol.* 206, *pp.* 477–496
Printed in Great Britain

On the lengthscales of laminar shock/boundary-layer interaction

By EDGAR KATZER†
Institute of Theoretical Fluid Mechanics, DLR-AVA, Bunsenstr. 10,
D-3400 Göttingen, FRG

(Received 3 July 1987 and in revised form 5 October 1988)

The interaction of an oblique shock with a laminar boundary layer on an adiabatic flat plate is analysed by solving the Navier–Stokes equations numerically. Mach numbers range from 1.4 to 3.4 and Reynolds numbers range from 10^5 to 6×10^5. The numerical results agree well with experiments. The pressure distribution at the edge of the boundary layer is proposed as a sensitive indicator of the numerical resolution. Local and global properties of the interaction region are discussed. In the vicinity of the separation point, local scaling laws of the free interaction are confirmed. For the length of the separation bubble a new similarity law reveals a linear influence of the shock strength. A comparison with the triple-deck theory shows that, for finite Reynolds numbers, the triple deck tends to overestimate the lengthscale substantially and that this discrepancy increases with increasing Mach number. The triple-deck model of displacing the main part of the boundary layer is substantiated by the numerical results. An asymmetrical structure within the separation bubble causes a characteristic distribution of the wall shear stress.

1. Introduction

Shock/boundary-layer interaction is a basic phenomenon of viscous–inviscid interaction. Because of its great importance in practice, for example its influence on the performance of transonic airfoils, supersonic air intakes, gas turbines and re-entry vehicles, it has been studied numerous times since the early investigations by Ackeret, Feldmann & Rott (1946) and Liepmann (1946). Reviews of experimental and theoretical investigations can be found in Stanewsky (1973), Hankey & Holden (1975), Kluwick (1979), Adamson & Messiter (1980) and Delery & Marvin (1986).

The present paper deals with the two-dimensional interaction of an oblique shock impinging on a laminar boundary layer at an adiabatic flat plate, figure 1. The boundary layer encountering the pressure increase p_3/p_1 across the interaction region is retarded and separates if the shock is sufficiently strong. An extensive upstream influence of the shock occurs (Liepmann, Roshko & Dhawan 1952). The impinging shock is reflected as an expansion fan, thus turning the flow towards the wall where the flow reattaches. A very flat and extended separation bubble results (note that the transverse scale is considerably stretched in figure 1). Two compression zones extending from the separation and reattachment region cause a pressure increase at the beginning and end of the interaction region enclosing a pressure plateau over the separation bubble. The wall shear stress decreases at the beginning of the interaction

† Present address: Institute for Informatics and Applied Mathematics, Christian-Albrechts-University, D-2300 Kiel, Federal Republic of Germany.

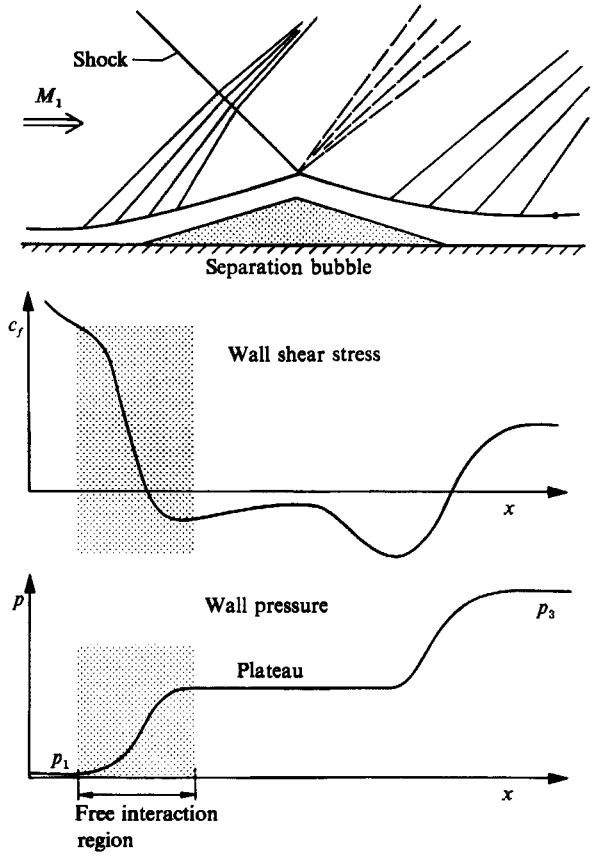

FIGURE 1. Oblique shock/laminar boundary-layer interaction.

region and increases in the reattachment region. Its shape in the reversed flow region will be discussed in the present paper.

Chapman, Kuehn & Larson (1958) have shown that the flow properties in the vicinity of the separation point are not dependent on the downstream boundary condition, i.e. the shock strength in the present case, and have introduced the term 'free interaction' for this phenomenon. Oswatitsch (see Oswatitsch & Wieghardt 1942) was the first to predict the free interaction as a self-induced mechanism between boundary layer and supersonic outer flow. A thickening of the boundary layer due to an initial disturbance deflects the supersonic flow. This generates a compression which again increases the boundary-layer thickness until frictional forces balance this unstable situation. For large Reynolds numbers, an asymptotic analysis shows that the interaction region exhibits a triple-deck structure; for details see the review of Stewartson (1974). For small disturbances of the order $Re^{-\frac{1}{4}}$, i.e. for weak shocks, the entire interaction region can be described by the triple deck. For this case Rizzetta, Burggraf & Jenson (1978) obtained triple-deck solutions for the flow field along a compression ramp on a flat plate. For stronger shocks a large separation region is established, the length of which tends to infinity with respect to the lengthscale of the triple deck. Burggraf (1975) estimated the lengthscales for this case. His analysis is based on the asymptotic structure of the reverse-flow region presented by Neiland (1971) and Stewartson & Williams (1973). Brown & Williams

(1975) extended the triple-deck analysis and included a higher-order term of the expansion.

The present paper analyses lengthscales and pressure scales of two-dimensional shock/boundary-layer interaction for finite Reynolds numbers. The influence of Reynolds number, Mach number and shock strength is investigated. The shock strengths are moderate to large with respect to the triple-deck scaling but the shocks are weak in the sense of small deflections of the inviscid flow field. The analysis is based on numerical solutions of the Navier–Stokes equations. The free interaction process will be analysed and details of the reverse-flow region will be shown.

2. Basic equations and evaluation of numerical influences

The numerical approach is based on the Navier–Stokes equations together with the continuity and the energy equation. For any given control volume $\mathscr{V}$, fixed in space, with surface $\partial\mathscr{V}$ (the term 'volume' is used here, although in the present two-dimensional case it is actually an area), these equations yield

$$\frac{\partial}{\partial t}\int_{\mathscr{V}} \rho \,\mathrm{d}V = -\int_{\partial\mathscr{V}} \rho(v\,\mathrm{d}s), \tag{1}$$

$$\frac{\partial}{\partial t}\int_{\mathscr{V}} \rho v \,\mathrm{d}V = -\int_{\partial\mathscr{V}} \rho v(v\,\mathrm{d}s) + \int_{\partial\mathscr{V}} S\,\mathrm{d}s, \tag{2}$$

$$\frac{\partial}{\partial t}\int_{\mathscr{V}} \rho e_{\mathrm{t}} \,\mathrm{d}V = -\int_{\partial\mathscr{V}} \rho e_{\mathrm{t}}(v\,\mathrm{d}s) + \int_{\partial\mathscr{V}} (Sv - q)\,\mathrm{d}s, \tag{3}$$

where ρ, ρv, ρe_{t} are density, momentum and total energy ($e_{\mathrm{t}} = e + \frac{1}{2}v^2$) per unit volume; S is the stress tensor, q is heat conduction and e is the internal energy. The fluid is assumed to be a perfect gas with ratio of specific heats $\gamma = 1.4$. For the viscous stress tensor the Newtonian viscosity law is assumed to have zero bulk viscosity (Stokes' hypothesis) and the shear viscosity μ to obey Sutherland's law

$$\frac{\mu}{\mu_\infty} = \left(\frac{T}{T_\infty}\right)^{\frac{3}{2}} \frac{T_\infty + T_{\mathrm{s}}}{T + T_{\mathrm{s}}} \tag{4}$$

with a non-dimensional Sutherland constant, T_{s}/T_∞, of 1/3. Heat conduction q is governed by Fourier's law with a constant Prandtl number of 0.72. The origin of the coordinate system is taken at the position x_0 where the incident shock would meet the plate in the inviscid case. The Reynolds number Re_{x_0} is based on the free stream conditions and the distance of x_0 from the leading edge. Lengthscales are normalized with the displacement thickness δ_0^* of an undisturbed flat-plate boundary layer at position x_0.

The governing equations are discretized using a rectangular non-equidistant grid (figure 2). Small grid spacings are applied on the wall and near the shock impingement point. The triple-deck theory characterizes the lengthscales of the separation and reattachment region. A sufficient resolution of the lower deck requires that the grid spacings on the wall satisfy the restrictions

$$\Delta y \leqslant Re_{x_{\mathrm{s}}}^{-\frac{1}{2}} \delta_0^*, \tag{5}$$

$$\Delta y \approx Re_{x_{\mathrm{s}}}^{-\frac{1}{2}} \Delta x, \tag{6}$$

where x_{s} is an *a priori* estimate of the separation point. Details of the grid distribution are given in Appendix A.

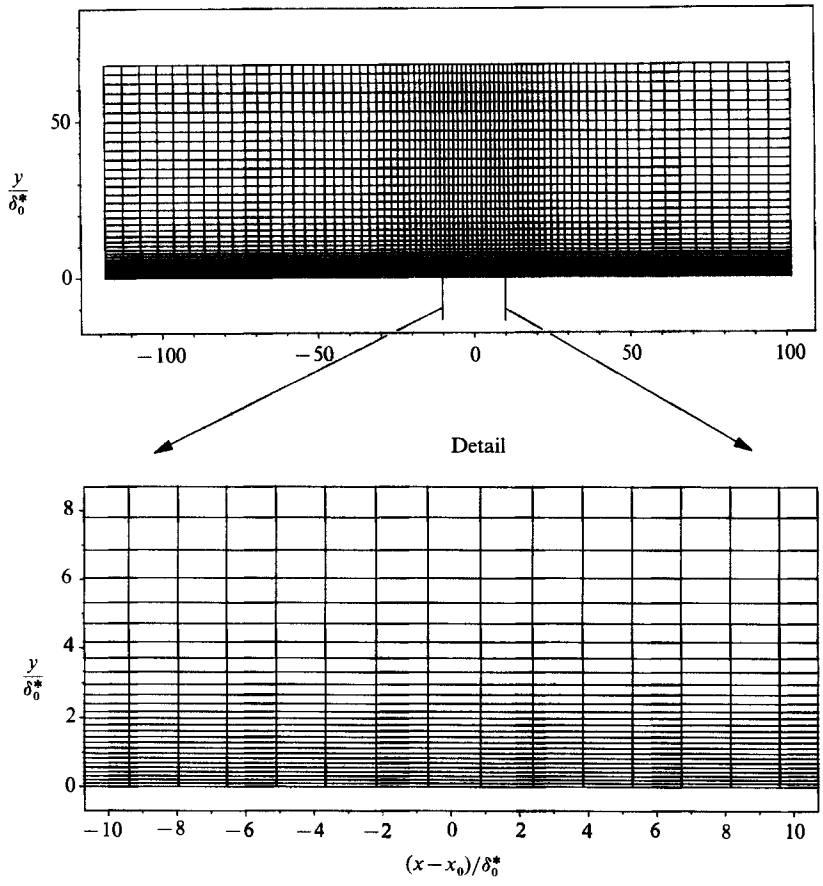

FIGURE 2. Computational grid and detail near shock impingement. (Notice that every second grid line is plotted.)

The inflow boundary is located some distance downstream of the leading edge. An undisturbed flat-plate boundary layer is prescribed at the inflow boundary. At the far-field boundary opposite the wall, undisturbed flow is applied upstream of the shock and the Rankine–Hugoniot values are specified behind the shock. Vanishing gradients

$$\frac{\partial}{\partial x}(\rho, \rho v, \rho e_t) = \frac{\partial^2}{\partial x^2}\rho u = 0 \tag{7}$$

are assumed at the outflow boundary. Adiabatic wall conditions and the no-slip boundary condition are applied on the wall. Furthermore, a vanishing pressure gradient, $\partial p/\partial y = 0$, is assumed on the wall. The error of this pressure condition has been estimated by analysing the wall shear-stress distribution and was found to be of the order 10^{-5} for the Reynolds numbers of the present investigation. Numerical tests confirmed that a variation of the boundary's location causes negligible disturbance of the interaction region as long as the boundaries are sufficiently far away from the interaction region. See Katzer (1985) for details.

The governing equations are solved by the explicit time-split MacCormack (1969) scheme; details are presented in Appendix B. Initial conditions are given by the inviscid case of a shock reflection on the wall. The calculation proceeds in time until

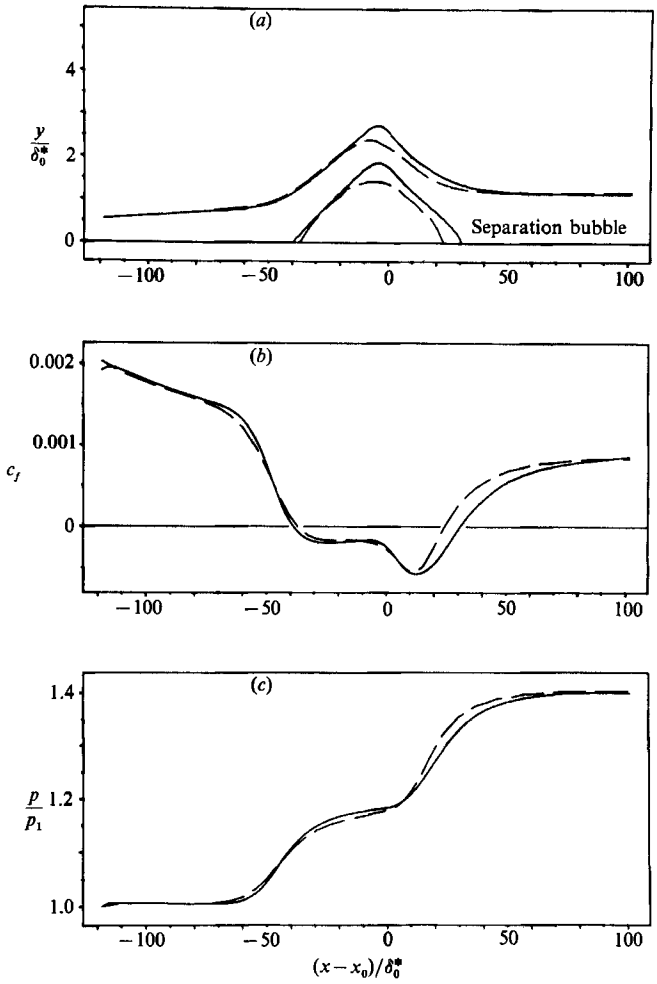

FIGURE 3. Influence of the grid size on the solution: – – –, 51 × 41 gridpoints; ——, 151 × 81 gridpoints, $\epsilon = 2.0$. (*a*) Displacement thickness, (*b*) wall shear stress, (*c*) wall pressure.

Grid size $N_x \times N_y$	Step sizes $\Delta x_{\min}/\delta_0^*$ $\Delta x_{\max}/\delta_0^*$	$\Delta y_{\min}/\delta_0^*$ $\Delta y_{\max}/\delta_0^*$	ϵ	δ_{SH}/δ_0^*	l_B/δ_0^*	h_B/δ_0^*
51 × 41	2.65	0.123	2.0	≈ 27	61.3	1.44
	7.85	3.602				
151 × 81	0.88	0.061	2.0	11	69.7	1.87
	2.66	1.792	0.5	6	69.6	1.92
192 × 103	0.70	0.047	0.4	3½	71.9	1.99
	2.09	1.403	0.1	2	71.8	2.00
151 × 101	0.76	0.048	0.5	3½	71.0	1.97
	2.96	1.429				

TABLE 1. Influence of grid size and numerical dissipation ϵ on numerical width of the shock at the edge of the boundary layer δ_{SH} and the length l_B and height h_B of the separation bubble. ($M_1 = 2.0$, $Re_{x_0} = 3 \times 10^5$, $p_3/p_1 = 1.4$.)

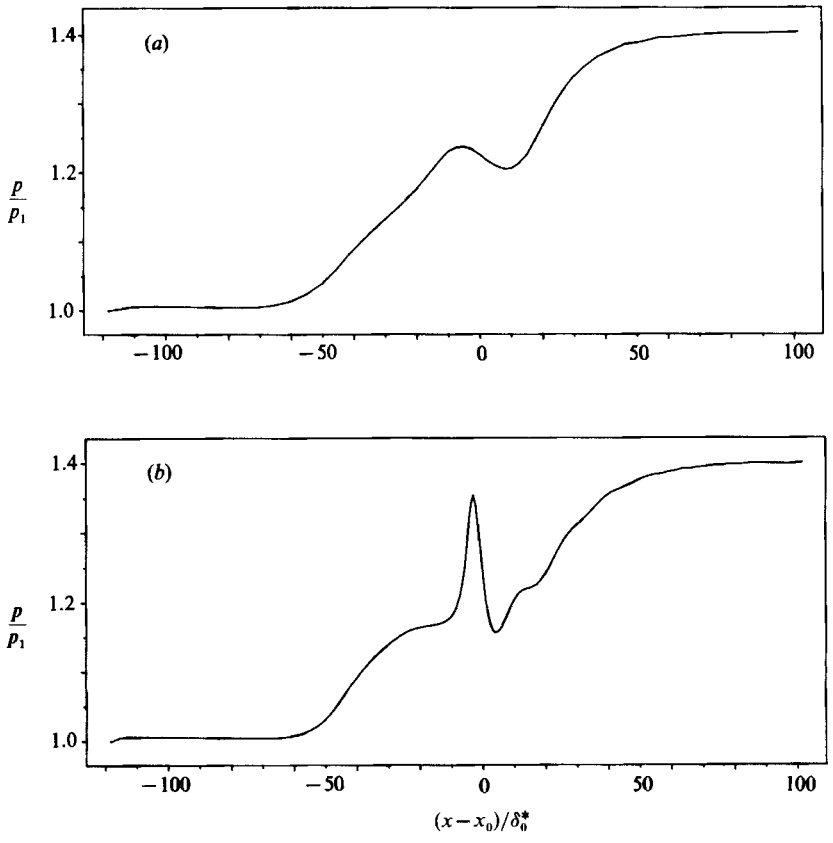

FIGURE 4. Pressure distribution at the edge of the boundary layer. (*a*) 51 × 41 grid, $\epsilon = 2.0$; (*b*) 151 × 101 grid, $\epsilon = 0.5$.

a steady state is reached. This is assumed when the root mean square of the wall pressure,

$$R(c_p) = \left(\frac{1}{N}\sum_{i=1}^{N}\left(\frac{c_p^{t+\Delta t}(x_i) - c_p^t(x_i)}{\Delta t}\right)^2\right)^{\frac{1}{2}}, \tag{8}$$

is smaller than 10^{-6}. Here, N is the number of grid points on the wall. The slowly growing length of the interaction region, l_{int}, controls the convergence. Non-dimensional convergence times are in the order of

$$t^{\infty} \approx (15 \ldots 35)\, l_{\text{int}}/U_{\infty}. \tag{9}$$

Typical computation times on a CRAY-1/S are 1 to 5 hours. The rate of data processing is 12 μs per grid point and time step. The numerical code is extremely fast and reaches a computational speed of 60×10^6 floating-point operations per second on a CRAY-1/S.

The influence of the grid on the numerical solution is analysed for the free-stream Mach number $M_1 = 2$, Reynolds number $Re_{x_0} = 3 \times 10^5$ and shock strength $p_3/p_1 = 1.4$. Results obtained with a coarse and a fine grid are compared in figure 3. The wall pressure curves and the wall shear-stress distributions agree with one another fairly well but there are differences in size and shape of the separation bubbles. The separation bubble for the coarse grid is 12% smaller and its height is 23% shorter than for the fine grid. A further decrease of the grid spacings with a 192 × 103 grid

increases the length of the separation bubble by 3% and its height by 7%. For various grids, the sizes of the separation bubbles are given in table 1. Figure 3 shows that the wall pressure is not suitable for assessing the accuracy of the numerical solution. The pressure at the edge of the boundary layer is more appropriate for that purpose. The impinging shock generates a pressure increase followed immediately by a steep pressure decrease caused by the expansion fan. Figure 4 shows that this pressure peak is not resolved sufficiently by the coarse grid; shock and expansion fan are diffused over several grid points. The boundary layer is not subject to an impinging discontinuity but a gradual pressure gradient and the size of the separation bubble is underestimated. This confirms Messina's (1977) result that small grid spacings are required not only transverse to the boundary layer but also in the longitudinal direction. The width of the impinging shock profile should be an order of magnitude smaller than the extent of the interaction region. The shock width which is estimated by using the gradient of the pressure profile at the edge of the boundary layer, is presented in table 1 for various grid sizes. During the investigation, it was found that a redistribution of the grid points and an increased number of nodes normal to the wall give a sharper shock profile. The pressure at the edge of the boundary layer for the resulting 151×101 grid is shown in figure 4. For this grid, the diagonals of the grid cells in the far field are virtually aligned with the impinging shock. (The parameters defining this grid are given in table 4, Appendix A.) The shock inclination and the thickness of the boundary layer depend on the flow parameters; therefore various grids with sizes of the order 151×101 were applied for the parameter studies of §3–5.

The influence of the numerical dissipation which is controlled by the parameter ϵ will now be discussed. Table 1 shows that an increase of the dissipation by factor of 4 for a fixed grid has no influence on the length of the separation bubble and only a small influence on its height. Decreasing dissipation also decreases the numerical diffusion of the shock but increases numerical oscillations downstream of the shock impingement point. A dissipation parameter of $\epsilon = 0.5$ has been found to be a good compromise between a sufficient damping of numerical distortions and a sharp shock profile.

3. Comparison with experiments and details of the separation bubble

Figures 5 and 6 compare the numerical results for the free-stream Mach number $M_1 = 2$, Reynolds number 3×10^5 (slightly different from experimental conditions) and shock strength $p_3/p_1 = 1.25$ and 1.4 with the experiments conducted by Hakkinen *et al.* (1959). The wall pressure distributions and the boundary-layer profiles are in good agreement with the experiments. The wall shear stress agrees well for the weaker shock. For the stronger shock, there are considerable differences in the reattachment region. The length of the separation bubble is overestimated compared to the experiment. These discrepancies are somewhat surprising when the good agreement in the wall pressure distribution is taken into account. It was suspected that the differences between the lengthscales of experiment and calculation are due to the free-stream temperature of 320 K (i.e. $T_s/T_\infty = 0.33$) used in the calculation and which is expected to be too high compared with the experiment. As a consequence, computations were performed with a free-stream temperature of 160 K. This halving of the free-stream temperature reduced the length of the separation bubble by only 3%, so that the differences between the numerical calculation and the experiment could not be attributed to temperature effects. The

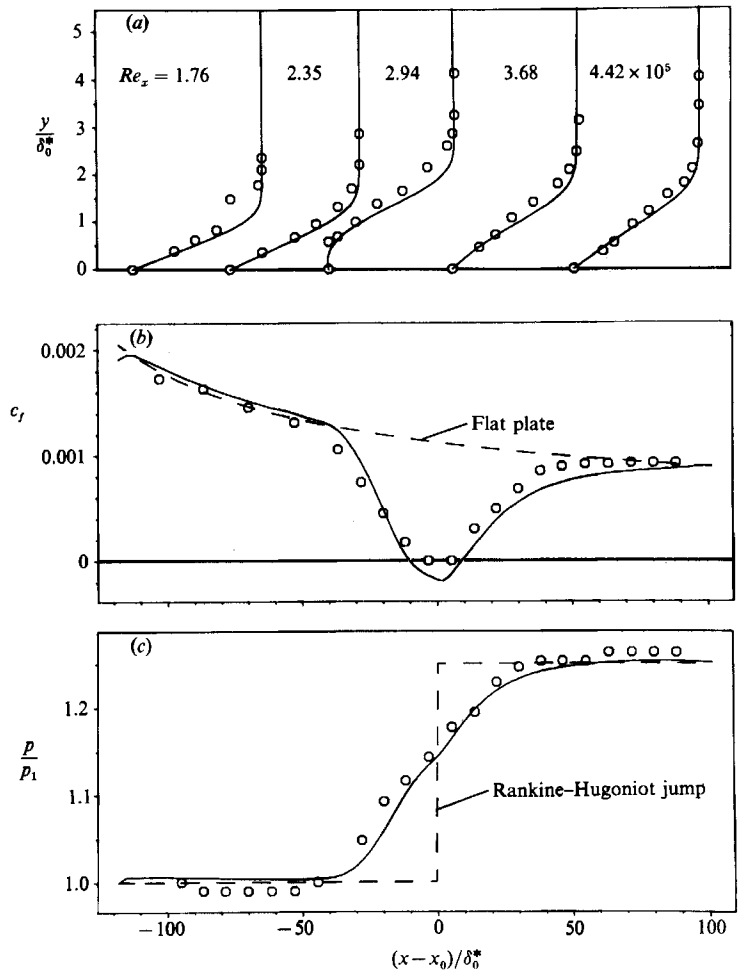

FIGURE 5. Comparison of numerical solution with experiment. $M_1 = 2.0$, $Re_{x_0} = 3 \times 10^5$, $p_3/p_1 = 1.25$, ——, numerical solution; ○, experiment: Hakkinen *et al.* (1959). (*a*) Boundary-layer profiles at station x; (*b*) wall shear stress; (*c*) wall pressure.

experimental value of the final pressure p_3 seems to be slightly below the quoted value of 1.4. A comparison of the numerical results for a shock strength of 1.375 with the experiment shows very good agreement with the wall shear stress up to separation but the length of the separated region is still overestimated considerably. In the experimental investigations, the wall shear stress has been measured using a Stanton probe contacting the wall. This disturbance of the boundary layer could have influenced the length of the separation bubble. In addition, the two experimental values with zero wall shear stress indicate that no positive value of the wall shear stress has been detected. They are located well within the separation bubble and cannot be used to determine the actual bubble length.

Figure 7 shows streamlines in the boundary layer and within the separation bubble. Note that the vertical scale is magnified by a factor of about ten. In the present case, the separation bubble exhibits a symmetrical triangular shape. It is surprising that an asymmetrical structure is found within the bubble despite this external symmetry. The centre region with the fluid at rest is shifted to the right

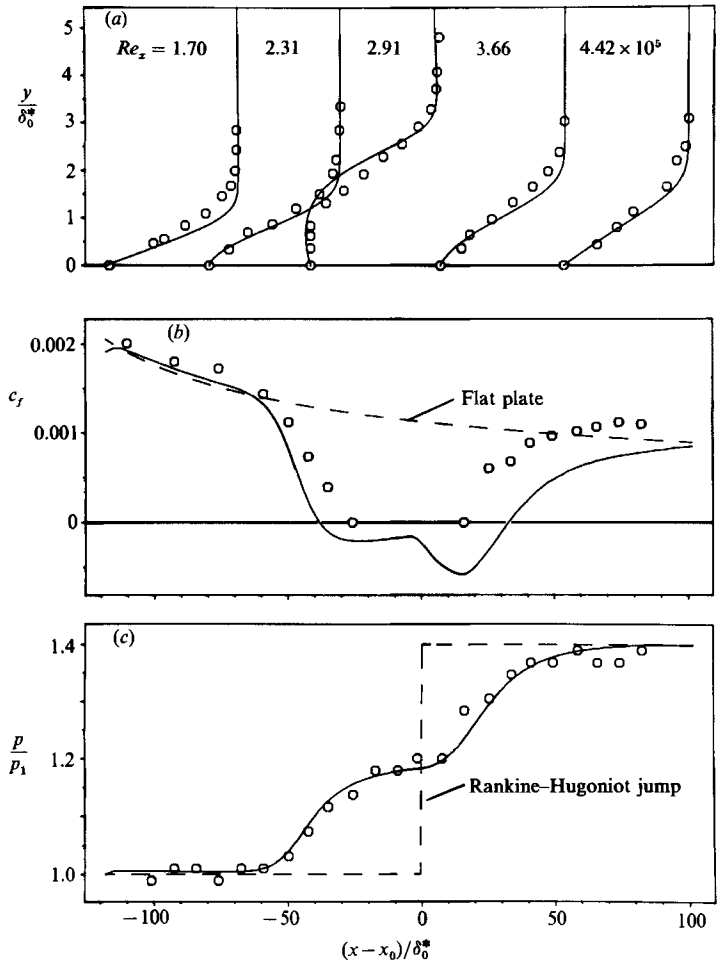

FIGURE 6. Comparison of numerical solution with experiment. $M_1 = 2.0, Re_{x_0} = 3 \times 10^5, p_3/p_1 = 1.4$, ——, numerical solution; ○, experiment: Hakkinen *et al.* (1959). (*a*) Boundary-layers profiles at station x; (*b*) wall shear stress; (*c*) wall pressure.

beneath the falling flank of the bubble. The displacement of this centre generates the typical shape of the wall shear-stress curve: a second minimum occurs just before reattachment. The author has found this second minimum in all of his numerical results except for very small separation bubbles. An inspection of published sources discloses that such a second minimum has also been obtained with various methods (Navier–Stokes calculations, inverse boundary-layer methods, triple-deck solutions) used by the following authors: Reyhner & Flügge-Lotz (1968), Skoglund & Gay (1969), Carter (1972), MacCormack & Baldwin (1975), Rizzetta *et al.* (1978), Peyret & Viviand (see Le Balleur, Peyret & Viviand 1980), MacCormack (1982), Bodonyi & Smith (1986), Degrez, Boccadoro & Wendt (1987), whereas it does not exist in the results obtained by MacCormack (1971), Li (1976), Wagner & Schmidt (1978), Beam & Warming (1978) and Haase, Wagner & Jameson (1984). The triple-deck analysis by Cebeci, Keller & Williams (1979) shows a similar asymmetrical structure within the separation bubble; see Stewartson (1981).

Consider now the streamlines within the approaching boundary layer. There are

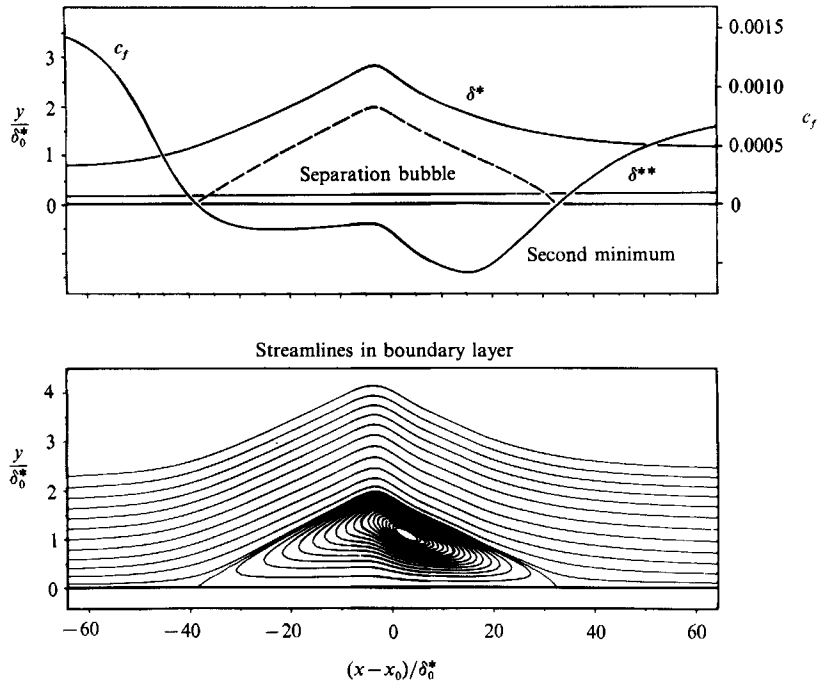

FIGURE 7. Streamlines within the separation bubble and in the boundary layer and wall shear-stress distribution, displacement thickness δ^* and momentum thickness δ^{**} in the interaction region. ($M_1 = 2.0$, $Re_{x_0} = 3 \times 10^5$, $p_3/p_1 = 1.4$.)

no significant disturbances in the streamline spacings as they pass through the interaction region. The oncoming boundary layer is simply displaced from the wall by the separation bubble. This resembles the free interaction model of the triple-deck theory with which the flow in the middle deck is displaced by the flow in the lower deck. For further verification, the variation of the displacement thickness and the momentum thickness across the interaction region has been analysed (figure 7). While the displacement thickness changes considerably in the interaction region, the momentum thickness is almost constant (in fact it increases slightly just like that of an undisturbed boundary layer). This again confirms the model of a displacement of the boundary layer by very slow fluid at the wall and slowly recirculating fluid within the separation bubble.

4. The free interaction region

A comprehensive investigation has been performed to verify whether the numerical solutions are able to confirm the local properties of the free interaction region at the separation point. For the various Mach numbers, Reynolds numbers and shock strengths given in table 2, shock/boundary-layer interactions were calculated. Table 2 provides the key to the symbols used in figures 8, 9 and 11. The pressure ratio p_3/p_1 across the incident and reflected shock in the inviscid case is used to measure the shock strength, whereas the weak interaction between the boundary layer and the outer flow field upstream of the shock/boundary-layer interaction region is neglected.

Symbol	Mach number M_1	Reynolds number Re_{x_0}	Shock strength p_3/p_1			
▲	1.414	10^5	1.20	1.25		
●	2.0	10^5	1.25	1.30	1.40	1.50
△	1.6	3×10^5	1.20	1.30	1.35	1.40
○	2.0	3×10^5	1.20	1.25	1.30	1.375
			1.40	1.50		
▽	2.8	3×10^5	1.60			
◇	3.4	3×10^5	1.60	1.644	1.80	
◓	2.0	6×10^5	1.40			

TABLE 2. Key to symbols in figures 8, 9, and 11: parameter combinations of numerical investigation

For the pressure at the separation point, p_s, the local scaling laws presented for example by Chapman *et al.* (1958), and Stewartson (1974) yield

$$c_{p_s} = \frac{2}{\gamma M_1^2}\frac{p_s - p_1}{p_1} = P_s[c_{f_1}/(M_1^2-1)^{\frac{1}{2}}]^{\frac{1}{2}}, \tag{10}$$

where c_{f_1} is the wall shear stress at the beginning, x_1, of the interaction region:

$$c_{f_1} = \frac{0.664}{(Re_{x_1}/C)^{\frac{1}{2}}} \tag{11}$$

and

$$C = \frac{\mu_w}{\mu_\infty}\frac{T_\infty}{T_w} \tag{12}$$

is the Chapman–Rubesin constant. The value of the constant P_s given by various authors varies within the range from 1.15 to 1.45. An analogous scaling law applies for the plateau pressure with a different constant P_p. Figure 8 shows the pressure at the separation point and the plateau pressure of the numerical calculations plotted according to the scaling law (10). For the pressure at separation this law is confirmed by the calculations which yield a constant of $P_s = 1.4$. Analogous results are obtained for the plateau pressure with constant $P_p = 2.3$. The scatter of these data indicates that the pressure plateau is not fully developed for weak shocks. The pressure constants are in good agreement with the experimental data of Greber, Hakkinen & Trilling (1958) and Hakkinen *et al.* (1959), which yield $P_s = \sqrt{2}$, $P_p = 2.33$, and the triple-deck scaling which yields $P_s = 1.45$ (Stewartson & Williams 1969) and $P_p = 2.55$ (Williams 1974).

To examine the length of the free interaction region, the distance l_s between the beginning of the interaction region and the separation point has been analysed. The beginning of the interaction region is determined by intersecting the tangent on the wall pressure curve at separation with the abscissa. The free interaction length l_s is scaled with a local reference value, namely the displacement thickness δ_s^* of an

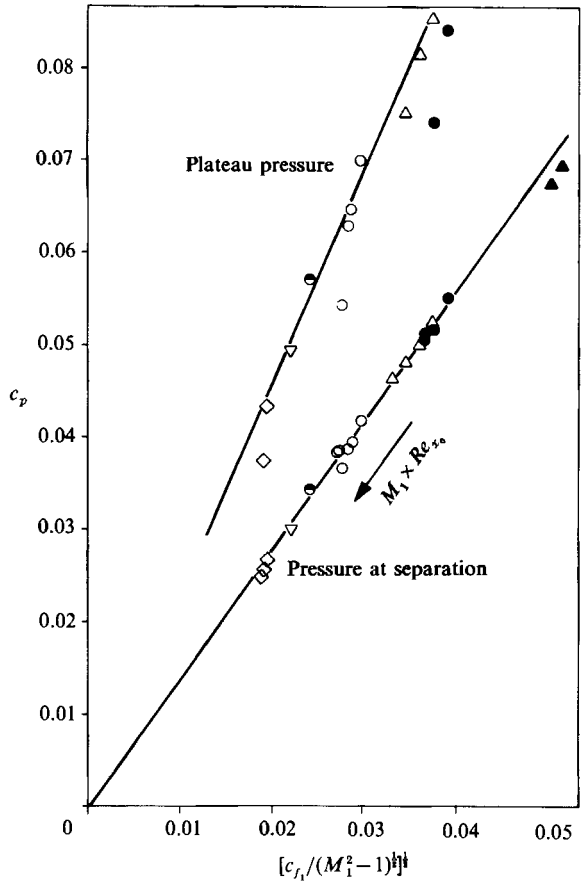

FIGURE 8. Pressure at separation point and plateau pressure. See table 2 for legend of symbols.

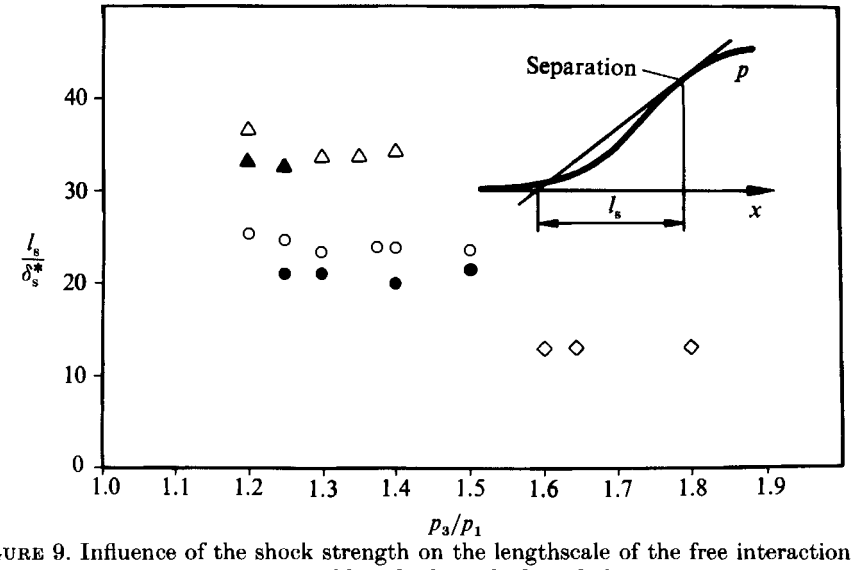

FIGURE 9. Influence of the shock strength on the lengthscale of the free interaction region. See table 2 for legend of symbols.

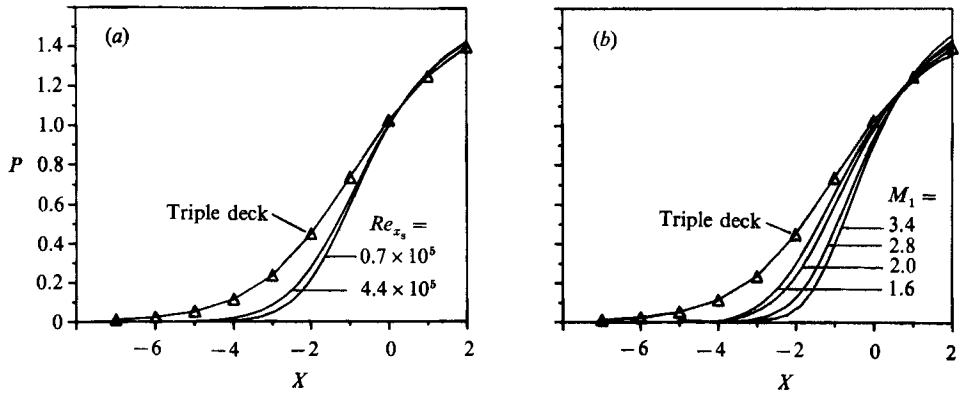

FIGURE 10. Comparison of Navier–Stokes solutions with the triple-deck theory. Wall pressure near separation point: (*a*) for various Reynolds numbers, $M_1 = 2.0$; and (*b*) for various Mach numbers, $Re_{x_s} \approx 2.4 \times 10^5$

undisturbed flat-plate boundary layer at the position x_s where separation will take place:

$$\delta_s^* = \frac{x_s}{(Re_{x_s}/C)^{\frac{1}{2}}}\left(1.72 + 2.22\frac{\gamma-1}{2}M_1^2\right). \tag{13}$$

Figure 9 shows the influence of the shock strength on the free interaction length. The free interaction property is obvious: its length l_s is independent of the shock strength, instead it depends only on the local flow conditions, eg. δ_s^*, in the vicinity of the separation point. There are only indirect influences of the shock which determine whether and where separation takes place, thereby determining the local flow conditions in the vicinity of the separation point.

A comparison between the present Navier–Stokes calculations and the result of the triple-deck theory is shown in figure 10. Figure 10(*a*) shows the wall pressure in the vicinity of the separation point for two finite Reynolds numbers. The Mach number is 2.0, wall temperature is $1.68T_\infty$ and the Chapman–Rubesin constant is 0.86. Wall pressure and lengthscale are expressed as non-dimensional triple-deck variables (Stewartson 1974):

$$X = \frac{x-x_s}{x_s}[(M_1^2-1)Re_{x_s}/C]^{\frac{3}{8}}\,(T_w/T_\infty)^{-\frac{3}{2}}\lambda^{\frac{1}{2}}, \tag{14}$$

$$P = \frac{p-p_1}{p_1}[(M_1^2-1)Re_{x_s}/C]^{\frac{1}{4}}\frac{1}{\gamma M_1^2}\lambda^{-\frac{1}{2}}, \tag{15}$$

where λ is 0.332.

As the wall pressure curves show, the triple-deck solution tends to overestimate the lengthscale for finite Reynolds numbers. With increasing Reynolds number, this discrepancy is reduced but the Reynolds numbers of the numerical calculation are still far too low to show good agreement with the asymptotic theory. The trend that the triple deck tends to overestimate the lengthscale has also been confirmed by Burggraf (1975) in comparison with experiments and by Burggraf *et al.* (1979) in comparison with interacting boundary-layer theory. In the latter case good agreement with the triple deck was achieved for extremely large Reynolds numbers of about 10^9, where an asymptotic theory might be expected to become more accurate.

As figure 10 (*b*) shows, the discrepancy between the Navier–Stokes solution and the triple-deck solution increases with increasing Mach numbers. The Mach number varies between 1.6 and 3.4 whereas the Reynolds numbers (based on x_s) are of about the same order of 2.4×10^5. It is interesting that all pressure curves cross at nearly one single point near the separation point. This explains the good agreement between the present Navier–Stokes solution and the triple-deck theory for the pressure at the separation point.

5. Length of the separation bubble

The length of the separation bubble is discussed here as a global lengthscale of the interaction region. Figure 11 (*a*) shows the influence of Mach number, Reynolds number and shock strength on the length of the separation bubble l_B scaled with δ_0^*. The bubble length increases with increasing shock strength p_3/p_1. The intersections of the plotted lines with the abscissa show that separation occurs when the shock strength is larger than a certain threshold value. This shock strength for incipient separation, p_{inc}, can be scaled according to the laws of the free interaction:

$$\frac{p_{inc}-p_1}{p_1} = \tfrac{1}{2}\gamma M_1^2 P_{inc}\,[c_{f_0}/(M_1^2-1)^{\frac{1}{2}}]^{\frac{1}{2}}, \tag{16}$$

where c_{f_0} is the wall shear stress of an undisturbed flat-plate boundary layer at shock impingement x_0. The constant P_{inc} is determined from figure 11 (*a*) to be

$$P_{inc} = 1.85\sqrt{2}, \tag{17}$$

whereas experimental and theoretical analyses by Greber *et al.* (1958) yield $P_{inc} = 2\sqrt{2}$ and triple-deck results by Rizzetta *et al.* (1978) yield $P_{inc} = 1.57\sqrt{2}$. Keeping in mind the experimental difficulties to discover very small separation bubbles, the comparison of the numerical computation with experiment is very good.

The influence of Mach and Reynolds number on the length of the separation bubble can be seen clearly in figure 11 (*a*). Increasing the Reynolds number and decreasing the Mach number increases the bubble length. An appropriate Mach and Reynolds number scaling leads to a new similarity law for the length of the separation bubble:

$$\frac{l_B}{\delta_0^*}\frac{M_1^3}{(Re_{x_0}/C)^{\frac{1}{2}}} = 4.4\frac{p_3-p_{inc}}{p_1}. \tag{18}$$

Figure 11 (*b*) shows the length of the separation bubble plotted with respect to this scale. All numerical data are described well by this similarity law. The factor $M_1^3/(Re_{x_0}/C)^{\frac{1}{2}}$, which is the same as the viscous–inviscid interaction parameter for hypersonic flows, should not be confused with the latter parameter because the present calculations are restricted to the supersonic range $1.4 \leqslant M_1 \leqslant 3.4$.

The Mach-number scaling has not been interpreted physically. It was chosen merely because it best fits the numerical data of the present investigation. For a thorough physical interpretation, an analysis of the influence of the wall temperature is recommended. In the present analysis with isolated wall conditions, the wall temperature depends on the Mach number and thus the effects of both parameters could not be separated. A crude interpretation of the Reynolds-number scaling can be made. Assuming that, once the shock strengths increase the threshold value for incipient separation, the pressure forces are balanced by friction forces along the separation bubble, it follows that $l_B Re_{x_0}^{-\frac{1}{2}}$ is independent of the Reynolds number, which yields the Reynolds-number scaling of (18).

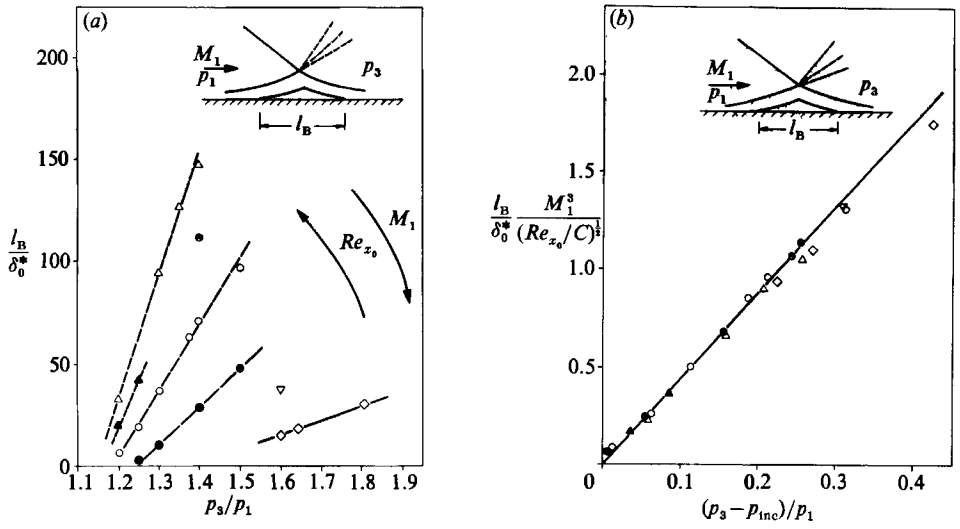

FIGURE 11. Length of the separation bubble. See table 2 for legend of symbols. (a) Influence of the shock strength. (b) Similarity law for the length of the separation bubble.

Mach number M_1	Reynolds number Re_{x_0}	Shock strength p_3/p_1	Length of separation bubble l_B/x_0	Length of separation bubble Triple-deck scale X_B
2.0	10^5	1.40	0.29	4.1
2.0	3×10^5	1.30	0.22	4.7
2.0	6×10^5	1.25	0.19	5.1
1.4	3×10^5	1.20	0.32	6.0
2.0	3×10^5	1.30	0.22	4.7
3.4	3×10^5	1.61	0.18	2.8
Length of separation bubble of triple-deck solution equivalent to all cases above is:				12.4

TABLE 3. Comparison of the length of the separation bubble with the triple-deck analysis by Rizzetta *et al.* (1978)

The present scaling law (18) for the length of the separation bubble is compared with the triple-deck solution by Rizzetta *et al.* (1978) who studied the shock/boundary-layer interaction induced by a compression ramp at the wall. It is assumed that the bubble length in this case is comparable with the bubble length of the present calculation, provided that the increases of pressure across the interaction region is the same in both cases. The length of the separation bubble given by the triple-deck analysis is obtained from figure 2 in Rizzetta *et al.* (1978) and yields $X_{TD} = 12.4$ for a non-dimensional ramp angle of 3. Table 3 shows the corresponding bubble length of the present investigation for an equivalent shock length. As different combinations of Mach and Reynolds numbers lead to the same triple-deck lengthscale, a variety of these parameters was chosen for comparison. No Navier–Stokes calculations were obtained for these specific parameter combinations. Instead, the similarity law (18), which in fact interpolates the Navier–Stokes

calculations, was used to calculate the length of the separation bubble. Scaling the bubble length according to (14) yields the triple-deck lengths X_B in table 3. In the same way as the triple-deck solution overestimates lengths in the vicinity of the separation point, it overestimates the bubble length by a factor of two to almost five. Furthermore, for finite Reynolds numbers, the discrepancy between the Navier–Stokes analysis and the triple-deck analysis not only depends on the Reynolds number but increases with increasing Mach number as well.

Burggraf (1975) presents a scaling law for the length of the plateau region. The analysis is based on the asymptotic theory of Neiland (1971) and Stewartson & Williams (1973) which is valid for large Reynolds numbers and extensive plateau regions. In the present notation this scaling law yields

$$\frac{l_B}{\delta_0^*}\frac{M_1^3}{(Re_{x_0}/C)^{\frac{1}{2}}} = K_B(M_1)\left(\frac{p_3-p_{inc}}{p_1}\right)^{\frac{3}{2}}, \tag{19}$$

where

$$K_B(M_1) = 19\frac{(T_w/T_\infty)^{\frac{3}{2}}}{1.72+1.11(\gamma-1)M_1^2}. \tag{20}$$

Here the length of the plateau region is identified with the length of the separation bubble and p_{inc} is identified with the corresponding threshold value of Burggraf. In the range of the present investigation, function K_B varies only slightly between 11.4 and 14.2 and consequently, the similarity law (18) gives nearly the same Mach- and Reynolds-number scaling as Burggraf's analysis (19). The influence of the pressure increase is given by the power of 1.5 in Burggraf's equation (19); this contrasts with the linear influence identified in figure 11(*a*). A possible reason for these different pressure influences is that the present investigation is restricted to separation bubbles which are not large enough for application of the asymptotic theory. Furthermore, the Reynolds numbers are not sufficiently large. It is interesting to note that for a shock strength of $p_3-p_{inc} = 0.14p_1$, which corresponds to $M_1 = 2.0$, $Re_{x_0} = 3\times10^5$, $p_3/p_1 = 1.33$, the length given by (18) is identical with Burggraf's scale (19). A numerical investigation of the lengthscale of extremely large separation bubbles is left for future studies.

6. Conclusions

The interaction of an oblique shock with the laminar boundary layer on a thermally isolated flat plate has been analysed numerically. The Navier–Stokes equations were solved using the explicit MacCormack (1969) scheme. The pressure distribution at the edge of the boundary layer is found to be useful for the assessment of the numerical resolution. The width of the impinging shock profile is recommended to be an order of magnitude smaller than the extent of the interaction region. Consequently, small grid spacings are required along the wall and in the orthogonal direction. The numerical results agree well with experiments by Hakkinen *et al.* (1959).

The influence of the Mach number in the range from 1.4 to 3.4, Reynolds number in the range from 10^5 to 6×10^5 and shock strength in the range from 1.2 to 1.8 was investigated. The shock strength necessary for boundary-layer separation was determined. Scaling laws of the interaction region were investigated and the existence of two different mechanisms was confirmed: a global mechanism ruling the length of the separation bubble and a local mechanism ruling the free interaction region in the vicinity of the separation point. For the length of the separation bubble

a new similarity law has been derived by correlating the numerical results. Within the range of the present investigation, the length of the separation bubble depends linearly on the shock strength and the influences of Mach and Reynolds number are given by the powers of 3 and $\frac{1}{2}$, respectively. This represents a global scaling law. The numerical results confirm that the lengthscale of the free interaction region does not depend on the shock strength. The pressure at the separation point and the plateau pressure are governed by the wall shear stress at the beginning of the interaction region and the Mach number at the edge of the boundary layer. Thus local scaling laws were verified.

The asymptotic theory of the triple deck is confirmed for the pressure scaling, whereas the lengthscales could not be verified for the finite Reynolds numbers investigated here. For the length of the separation bubble as well as the extent of the free interaction region near the separation point, the triple-deck lengthscale tends to overestimate the extent of the interaction region considerably. This discrepancy increases with increasing Mach number and decreases with increasing Reynolds number. The triple-deck model of passive displacement of the main part of the boundary layer in the middle deck is substantiated by the numerical calculations.

The shape and structure of the separation bubble has been analysed and an asymmetrical flow structure has been found inside the bubble. This leads to an asymmetrical distribution of the wall shear-stress curve which exhibits a second minimum just upstream of reattachment.

Analysis of the influence of the wall temperature and the physical interpretation of the mechanisms determining the length of the interaction region are recommended as topics for further research.

This work was performed at the Institute of Theoretical Fluid Mechanics of the German Aerospace Research Establishment (DLR-AVA) in Göttingen. The author thanks Professor Dr-Ing. H. Oertel, Institute of Theoretical Fluid Mechanics and Professor Dr-Ing. J. Zierep, Institute of Fluid Mechanics at the Technical University of Karlsruhe for many helpful discussions and for supporting this work. The valuable suggestions of the referees are gratefully acknowledged.

Appendix A. Distribution of the grid points

The numerical grid is generated by control functions which map equidistant nodes $\eta_i = i\,\Delta\eta$ upon non-equidistant nodes $y_i = f(\eta_i)$. The function which controls the node distribution in the y-direction is presented in the following paragraph. The nodes in the x-direction are generated similarly.

Control function f is assumed to be a strictly monotonic and continuously differentiable function and is uniquely defined by a few control nodes (η_k, y_k) and the slopes y'_k. The control function is defined within the interval $[\eta_k, \eta_{k+1}]$ either as a polynomial of degree three or as an exponential function. In the latter case, f is given locally as an affine transformation of the normalized function:

$$g(\xi) = \frac{e^{\alpha\xi} - 1}{e^{\alpha} - 1} \tag{A 1}$$

on the unit interval. Parameter α is determined by the slope y'_κ at one edge, κ, of the control interval:

$$\kappa = \begin{cases} k & \text{if} \quad y'_k < y'_{k+1} \\ k+1 & \text{if} \quad y'_k > y'_{k+1} \end{cases}. \tag{A 2}$$

y-distribution					x-distribution				
Function	k	η_k	y_k	y'_k	Function	k	η_k	x_k	x'_k
Polynomial	1	0	0	0.338	Exponential	1	0	−118.36	3.896
Exponential	2	4	2.03	0.676	Polynomial	2	32	−33.82	1.691
Polynomial	3	8	10.99	5.281	Polynomial	3	62	0.00	1.015
	4	14	67.64	10.145	Exponential	4	92	33.82	1.691
						5	115	101.45	4.692

TABLE 4. Control nodes defining the numerical grid. Case $M_1 = 2.0$, $Re_{x_0} = 3 \times 10^5$, $p_3/p_1 = 1.4$. Grid size is 151×101, leading edge of plate: $x_{LE} = -169.1$.

Table 4 defines the 151×101 grid used by the numerical calculation for the parameter case $M_1 = 2.0$, $Re_{x_0} = 3 \times 10^5$, $p_3/p_1 = 1.4$. Grids which have been used for other parameter combinations, are available from the author.

Appendix B. Numerical algorithm

In this section a concise definition of the numerical algorithm is presented; see Katzer (1985) for a comprehensive presentation. A shorthand notation of the governing equations (1)–(3) is introduced:

$$\frac{\partial}{\partial t}\int_{\mathscr{V}} U = \int_{\partial\mathscr{V}} H\,\mathrm{d}s, \tag{B 1}$$

and these equations are discretized for small control volumes which are defined using a rectangular grid (x_j, y_i). A control volume, identified by the indices (i, j), is defined by its vertices which are located at the centre of four adjacent grid nodes. A time-split finite-volume version of the MacCormack (1969) scheme (see MacCormack & Baldwin 1975) is given here as a sequence of operators, each dealing with only one direction of the flow field. The predictor operator in the J-direction, P_j, is given by the forward Euler discretization of the time derivative of (B1) thereby neglecting the fluxes in the I-direction through the cell surfaces $(i+\frac{1}{2}, j)$ and $(i-\frac{1}{2}, j)$:

$$P_J(U)_{ij} = U_{ij} + \frac{\Delta t}{\mathscr{V}_{ij}} \Delta y_{ij} (H^P_{i,j+\frac{1}{2}} - H^P_{i,j-\frac{1}{2}}) \tag{B 2}$$

Here $\mathscr{V}_{ij}$ is the area and Δy_{ij} is the length of the sides of the control volume. The fluxes in the J-direction, $H^P_{i,j+\frac{1}{2}}$, are given below. The corrector step in J-direction is defined in a similar way:

$$C_J(U)_{ij} = U_{ij} + \frac{\Delta t}{\mathscr{V}_{ij}} \Delta y_{ij} (H^C_{i,j+\frac{1}{2}} - H^C_{i,j-\frac{1}{2}}). \tag{B 3}$$

An averaging operator which will be denoted by an overbar yields a second-order accurate discretization of (B1):

$$\overline{C_J P_J}(U)_{ij} = \frac{1}{2}(U_{ij} + C_J P_J(U)_{ij}). \tag{B 4}$$

Predictor and corrector operators in the I-direction are defined in a similar manner where i and j are interchanged and Δy is replaced by Δx. Fourth-order numerical dissipation is introduced by the operators:

$$D_J(U)_{ij} = U_{ij} + \tfrac{1}{2}\epsilon \frac{|p_{ij-1} - 2p_{ij} + p_{ij+1}|}{p_{ij-1} + 2p_{ij} + p_{ij+1}} (U_{ij-1} - 2U_{ij} + U_{ij+1}), \tag{B 5}$$

and D_I which is defined similarly. The order of the operators is reversed every second time step which yields a symmetrical scheme proceeding the solution from time t to $t+2\Delta t$:

$$U^{t+2\Delta t} = D_J D_I \overline{P_I C_I P_J C_J} \overline{C_J P_J C_I P_I} (U^t). \tag{B 6}$$

The time step is restricted by the CFL condition given by MacCormack & Baldwin (1975). The entries in the flux tensors $H^P_{i,j+\frac{1}{2}}$ and $H^C_{i,j+\frac{1}{2}}$ are defined below for the operators in the J-direction. The pressure is

$$p_{i,j+\frac{1}{2}} = p_{i,j+e} \tag{B 7}$$

and the convective fluxes are given by

$$(Uv^{\mathrm{T}})_{i,j+\frac{1}{2}} = \begin{cases} U_{i,j+e}\, v^{\mathrm{T}}_{i,j+e} & \text{otherwise} \\ U_{i,j+e}\, \frac{1}{2}(v^{\mathrm{T}}_{i,j} + v^{\mathrm{T}}_{i,j+1}) & \text{if } u_{i,j+1} \geqslant u_{i,j} \end{cases}, \tag{B 8}$$

where the indicator e is 1 for the predictor step and e is 0 for the corrector step. The superscript T denotes the row vector of the velocities and u denotes the velocity component in the x-direction. The author's experience suggests that the flux correction, which is in effect when the if-condition in (B8) is true, is not necessary for the I-operators in the y-direction normal to the wall. The construction of the viscous terms in the stress tensor is given by Deiwert (1975).

REFERENCES

Ackeret, J., Feldmann, F. & Rott, N. 1946 Untersuchungen an Verdichtungsstößen und Grenzschichten in schnell bewegten Gasen. *Mitt. Inst. f. Aerodynamik, ETH Zürich, Nr.* 10. (English transl.: *NACA TM* 1113, 1947.)

Adamson, T. C. & Messiter, A. F. 1980 Analysis of two-dimensional interactions between shock waves and boundary layers. *Ann. Rev. Fluid Mech.* **12**, 103–138.

Beam, R. M. & Warming, R. F. 1978 An implicit factored scheme for the compressible Navier–Stokes equations. *AIAA J.* **16**, 393–402.

Bodonyi, R. J. & Smith, F. T. 1986 Shock-wave laminar boundary layer interaction in supercritical transonic flow. *Computers & Fluids* **14**, 97–108.

Brown, S. N. & Williams, P. G. 1975 Self-induced separation, III. *J. Inst. Maths. Applics.* **16**, 175–191.

Burggraf, O. R. 1975 Asymptotic theory of separation and reattachment of a laminar boundary layer on a compression ramp. *AGARD-CP* 168.

Burrggraf, O. R., Rizzetta, D. Ph., Werle, M. J. & Vatsa, V. N. 1979 Effect of Reynolds number on laminar separation of a supersonic stream. *AIAA J.* **17**, 336–343.

Carter, J. E. 1972 Numerical solutions of the Navier–Stokes equations for the supersonic laminar flow over a two-dimensional compression corner. *NASA TR* R-385.

Cebeci, T., Keller, H. B. & Williams, P. G. 1979 Separating boundary-layer flow calculations. *J. Comput. Phys.* **31**, 363–378.

Chapman, D. R., Kuehn, D. M. & Larson, H. K. 1958 Investigation of separated flows in supersonic and subsonic streams with emphasis on the effect of transition. *NACA Rep.* 1356.

Degrez, G., Boccadoro, C. H. & Wendt, J. F. 1987 The interaction of an oblique shock wave with a laminar boundary layer revisited. An experimental and numerical study. *J. Fluid Mech.* **177**, 247–263.

Deiwert, G. S. 1975 Numerical simulation of high Reynolds number transonic flows. *AIAA J.* **13**, 1354–1359.

Delery, J. & Marvin, J. G. 1986 Shock-wave boundary layer interactions. *AGARDograph* AG-280.

Greber, I., Hakkinen, R. J. & Trilling, L. 1958 Laminar boundary layer oblique shock wave interaction on flat and curved plates. *Z. Angew. Math. Phys.* **9b**, 312–331.

Haase, W., Wagner, B. & Jameson, A. 1984 Development of a Navier–Stokes method based on a finite volume technique for the unsteady Euler equations. *Fifth GAMM-Conf. on Numerical*

Methods in Fluid Dynamics, Rome 1983, Proceedings: Notes on Numerical Fluid Mechanics 7, pp. 99–107. Vieweg.

HAKKINEN, R. J., GREBER, I., TRILLING, L. & ABARBANEL, S. S. 1959 The interaction of an oblique shock wave with a laminar boundary layer. *NASA Memo* 2-18-59W.

HANKEY, W. L. & HOLDEN, M. S. 1975 Two-dimensional shock wave boundary layer interactions in high speed flows. *AGARDograph* AG-203.

KATZER, E. 1985 Numerische Untersuchung der laminaren Stoß-Grenzschicht-Wechselwirkung. *DFVLR-FB* 85–34. (English transl.: ESA-TT-958, 1986.)

KLUWICK, A. 1979 Stationäre, laminare wechselwirkende Reibungsschichten. *Z. Flugwiss. Weltraumforschung* **3**, 157–174.

LE BALLEUR, J. C., PEYRET, R. & VIVIAND, H. 1980 Numerical studies in high Reynolds number aerodynamics. *Computers Fluids* **8**, 1–30.

LI, C. P. 1976 A mixed explicit–implicit splitting method for the compressible Navier–Stokes Equations. Proc. *Fifth Intl Conf. on Numerical Methods in Fluid Dynamics, Enschede 1976*, Lecture Notes in Physics, vol. 59, pp. 285–292. Springer.

LIEPMANN, H. W. 1946 The interaction between boundary layer and shock waves in transonic flow. *J. Aeronaut. Sci.* **13**, 623–637.

LIEPMANN, H. W., ROSHKO, A. & DHAWAN, S. 1952 On reflection of shock waves from boundary layers. *NACA Rep.* **1100**.

MACCORMACK, R. W. 1969 The effect of viscosity in hypervelocity impact cratering. *AIAA Paper* 69–354.

MACCORMACK, R. W. 1971 Numerical solution of the interaction of a shock wave with a laminar boundary layer. *Proc. Second Intl. Conf. on Numerical Methods in Fluid Dynamics, Berkely 1970*, Lecture Notes in Physics, vol. 8, pp. 151–163. Springer.

MACCORMACK, R. W. 1982 A numerical method for solving the equations of compressible viscous flow. *AIAA J.* **20**, 1275–1281.

MACCORMACK, R. W. & BALDWIN, B. S. 1975 A numerical method for solving the Navier–Stokes equations with application to shock-boundary layer interactions. *AIAA Paper* 75–1.

MESSINA, N. A. 1977 A computational investigation of shock waves, laminar boundary layers and their mutual interaction. Ph.D. thesis Department of Aerospace and Mechanical Science, School of Engineering and Applied Science, Princeton University.

NEILAND, V. YA. 1971 Flow behind the boundary layer separation point in a supersonic stream. *Izv. Akad. Nauk SSSR, Mekh. Zhid. i Gaza* **3**, 19–21. (English transl.)

OSWATITSCH, K. & WIEGHARDT, K. 1942 Theoretische Untersuchungen über stationäre Potentialströmungen und Grenzschichten bei hohen Geschwindigkeiten. *Lilienthal-Bericht* S13/1, pp. 7–24. (English transl.: *NACA TM* 1189, 1948.)

REYHNER, T. A. & FLÜGGE-LOTZ, I. 1968 The interaction of a shock wave with a laminar boundary layer. *Intl. J. Non-Linear Mech.* **3**, 173–199.

RIZZETTA, P. D., BURGGRAF, O. R. & JENSON, R. 1978 Triple-deck solutions for viscous supersonic and hypersonic flow past corners. *J. Fluid Mech.* **89**, 535–552.

SKOGLUND, V. J. & GAY, B. D. 1969 Improved numerical techniques and solution of a separated interaction of an oblique shock wave and a laminar boundary layer. *University of New Mexico, Bueau of Engineering Research, Rep.* ME-41 (69) S-068.

STANEWSKY, E. 1973 Shock–boundary layer interaction in transonic and supersonic flow. *Von Kármán Inst. for Fluid Dynamics*, Lecture Series 59.

STEWARTSON, K. 1974 Multistructured boundary layers on flat plates and related bodies. *Adv. Appl. Mech.* **14**, 145–239.

STEWARTSON, K. 1981 D'Alembert's Paradox. *SIAM Rev.* **23**, 308–343.

STEWARTSON, K. & WILLIAMS, P. G. 1969 Self-induced separation. *Proc. R. Soc. Lond.* A **312**, 181–206.

STEWARTSON K. & WILLIAMS, P. G. 1973 On self-induced separation II. *Mathematika* **20**, 98–108.

WAGNER, B. & SCHMIDT, W. 1978 Theoretische Untersuchungen zur Stoß-Grenzschicht-Wechselwirkung in kryogenem Stickstoff. *Z. Flugwiss. Weltraum.* **2**, 81–88.

WILLIAMS, P. G. 1974 A reverse flow computation in the theory of self-induced separation. *Proc. Fourth Intl Conf. on Numerical Methods in Fluid Dynamics*, Lecture Notes in Physics, vol. 35, pp. 445–451. Springer.